



# Mesoporous silica coating NaYF<sub>4</sub>:Yb,Er@NaYF<sub>4</sub> upconversion nanoparticles loaded with ruthenium(II) complex nanoparticles: Fluorometric sensing and cellular imaging of temperature by upconversion and of oxygen by downconversion

Sai Xu<sup>1</sup> · Yang Yu<sup>1</sup> · Yuefeng Gao<sup>2</sup> · Yanqiu Zhang<sup>1</sup> · Xiangping Li<sup>1</sup> · Jinsu Zhang<sup>1</sup> · Yunfeng Wang<sup>3</sup> · Baojiu Chen<sup>1</sup>

Received: 15 May 2018 / Accepted: 16 August 2018 / Published online: 12 September 2018  
© Springer-Verlag GmbH Austria, part of Springer Nature 2018

## Abstract

Accurate detection of temperature and oxygen concentration at the cellular level is important in tumor diagnosis. Multifunctional nanocomposites are described that consist of upconversion luminescent nanoparticles capped with mesoporous silica and loaded with an oxygen-sensitive luminescent ruthenium complex. The nanocomposites of type NaYF<sub>4</sub>:Yb,Er@NaYF<sub>4</sub>@mSiO<sub>2</sub>-Ru have two modes of operation: Its red downconversion luminescence (at excitation/emission peaks of 455/606 nm) is quenched by oxygen (O<sub>2</sub>), and this is used to sense and image O<sub>2</sub>. The green upconversion luminescence (typically acquired at excitation/emission wavelengths of 980/525 and 544 nm), in turn, is used to measure temperature. The nanocomposites were then applied to dual mode in-vitro imaging of temperature and O<sub>2</sub> in hepatocellular carcinoma cells (HepG-2).

**Keywords** Optical sensor · Dual sensor · Core-shell structure · Rare earth ions · Tumor diagnosis · Luminophore · HepG-2 · Thermal coupled levels

## Introduction

Cellular temperature and oxygen level are closely related to various diseases, including tumors, stroke and cardiovascular diseases [1]. Hyperthermia and hypoxia are the distinct features of tumors because of the tumor cell unlimited proliferation [2]. Therefore, measuring temperature and dissolved

oxygen in living cells are vitally important and necessary to tumor diagnose and subsequent treatments guidance. Unfortunately, the internal temperature and oxygen levels of the living cell cannot be detected via traditional contact measurement. Thus, it is indeed necessary to find a non-contact method to read out the internal temperature and oxygen concentration of the living cell.

Many temperature-sensitive luminescence materials have aroused much attention [3]. Among them, lanthanide doped upconversion nanocrystals are thought to be suitable and prospective as temperature sensors due to their unique optical properties such as large anti-Stokes shift, sharp emission lines and long lifetime. The excitation of near infrared (NIR) meets the biological penetration window leading to high penetration depth in tissues, high signal-to-noise ratio and absence of auto fluorescence from biological samples. These advantages ensure the upconversion fluorescent probe safely employed in the bio-sensing field [4]. Upconversion temperature sensors are mainly based on the temperature inducing fluorescence intensity ratios [5]. In this way, two thermal coupled levels of lanthanide ions are necessary. For Er<sup>3+</sup> ions, the distinctive green emission levels (<sup>2</sup>H<sub>11/2</sub> and <sup>4</sup>S<sub>3/2</sub>) are in thermal coupled regime [6]. Therefore, Yb<sup>3+</sup>/Er<sup>3+</sup> codoped upconversion nanoparticles (UCNPs) are ideal choice as thermal probe in living cells.

**Electronic supplementary material** The online version of this article (<https://doi.org/10.1007/s00604-018-2965-5>) contains supplementary material, which is available to authorized users.

✉ Yuefeng Gao  
yue232feng@163.com

✉ Baojiu Chen  
chenmbj@sohu.com

<sup>1</sup> College of Science, Dalian Maritime University,  
Dalian 116026, Liaoning, People's Republic of China

<sup>2</sup> Marine Engineering College, Dalian Maritime University,  
Dalian 116026, Liaoning, People's Republic of China

<sup>3</sup> School of Electronic and Electrical Engineering, Nanyang Institute of  
Technology, Nanyang 473061, Henan, People's Republic of China

As for oxygen sensing, several optical oxygen sensors have been reported because they offer advantages, including fast response, low toxicity, low cost, and high sensitivity [7, 8]. Several luminescent dyes have been used as oxygen probes. Among them, luminescent transition metal complexes, particularly those of Ru(II) complex, have been frequently exploited due to their long fluorescence lifetime and high sensitivity [9].

From the above analysis, it can be deduced that Yb<sup>3+</sup>/Er<sup>3+</sup> codoped upconversion nanocrystals and Ru(II) complex-based oxygen sensors both have crucial applications on biosensing. Thus, the design of the nanocomposites combining Ru complex with UCNPs is undoubtedly of great importance for establishing a novel multifunctional detection system in living cells. To achieve the nanocomposites used in biosensing, the key problem to be solved is the biocompatibility of UCNPs. Most of synthesis processes of UCNPs are accomplished in hydrophobic solvent such as oleic acid, oleylamine and 1-octadecene, so they need surface modifications for transferring to hydrophilia. Until now, several modification approaches have been exploited, including ligand exchange, ligand oxidization, and silanization [10]. Among these methods, mesoporous silica coating is currently a research hotpot due to its good compatibility. Furthermore, the high surface area of mesoporous silica layer provides a large target-receptor interface making the composites suitable for sensing applications [11].

Here, NaYF<sub>4</sub>:Yb,Er@NaYF<sub>4</sub> core-shell UCNPs were fabricated, and mesoporous silica shell was coated on UCNPs for hydrophilia, then the oxygen indicator ([Ru(dpp)<sub>3</sub>]<sup>2+</sup>Cl<sub>2</sub>) was loaded. The nanocomposites have two different modes of luminescence. The red downconversion luminescence (DCL) can be used to sense O<sub>2</sub>, and the green upconversion luminescence (UCL) is applied to detect temperature. In addition, they also own the function of dual-mode cell imaging with excitation of 980 nm and 455 nm under a confocal laser scanning microscopy (CLSM). In such a multifunctional sensing system, the temperature and oxygen-sensing properties are measured under different excitation wavelengths so that they do not disturb each other. Also, the advantages of the upconversion and downconversion emissions, such as low background fluorescence for Er<sup>3+</sup> and high luminescent efficiency for Ru complex, can be integrated into a system. What's more, the strategy to design multifunctional nanocomposites may be extended to prepare multifunctional platforms for various biosensing systems.

## Experimental

### Materials

1-Octadecene (ODE), oleic acid (OA), and [Ru(dpp)<sub>3</sub>]<sup>2+</sup>Cl<sub>2</sub> were purchased from Sigma-Aldrich (<https://www.sigmaaldrich.com/>). Tetraethyl orthosilicate (TEOS),

hexadecyl trimethyl ammonium bromide (CTAB), NaOH, NH<sub>4</sub>F, dimethyl sulfoxide (DMSO), YCl<sub>3</sub>·6H<sub>2</sub>O, YbCl<sub>3</sub>·6H<sub>2</sub>O, and ErCl<sub>3</sub>·6H<sub>2</sub>O were all obtained from Aladdin Industrial Corporation (<http://www.aladdin-e.com/>). All chemicals were used without further purification.

### Synthesis of NaYF<sub>4</sub>:Yb,Er@NaYF<sub>4</sub> upconversion nanoparticles (UCNPs)

NaYF<sub>4</sub>:Yb,Er nanoparticles and NaYF<sub>4</sub>:Yb,Er@NaYF<sub>4</sub> core-shell nanoparticles were synthesized according to the previously reported literatures [12]. The detailed description of the method is shown in the Electronic Supporting Material.

### Synthesis of UCNP@mSiO<sub>2</sub> nanocomposites

UCNP@mSiO<sub>2</sub> nanocomposites were synthesized according to a classical method with some modifications [13]. The corresponding description of the method is shown in the Electronic Supporting Material.

### Synthesis of multifunctional nanocomposites

5 mL of the UCNP@mSiO<sub>2</sub> nanoparticles (10 mg·mL<sup>-1</sup>) were mixed with 0.5 mL [Ru(dpp)<sub>3</sub>]<sup>2+</sup>Cl<sub>2</sub>/DMSO solution (1 mg·mL<sup>-1</sup>). The mixture was stirred in closed container in dark room for 24 h, the Ru complex loaded nanoparticles were separated by centrifugation and saved in phosphate buffered saline (PBS) (pH = 7.4) hermetically for future use.

### Cell cytotoxicity assay

In vitro cytotoxicity was evaluated by conducting MTT (3-(4,5-dimethylthiazol-2-yl)-2,5-diphenyltetrazolium bromide) assays. In a typical process, the cells were seeded onto 96-well plate for 24 h. After the cells attached to the plates, different concentrations of nanocomposite solution were incubated with the cells in 5% CO<sub>2</sub> at 37 °C for 24 h. At the end of the incubate time, 10 μL MTT solution (1 mg·mL<sup>-1</sup>) was added, and then the mixture solution was incubated for another 4 h. After that, the incubate medium was removed and 150 μL DMSO was added to each well. The absorbance of MTT was determined by a microplate reader (BioTek, ELX808, <https://www.biotek.com/>). A culture medium without the addition of NPs was regarded as control group. The cell viability was expressed as a percentage relative to the control group.

### Characterization

Size and morphology of the samples were obtained by a Hitachi H-800 transmission electron microscope (TEM) operating at an acceleration voltage of 200 kV (JEOL, <http://www.jeol.com/>).

jeol.com). The crystalline structures of the samples were characterized by X-ray diffraction (XRD) (Rigaku D/max-rA power diffractometer using Cu KR radiation ( $\lambda$ ) 1.54178 Å) (<https://www.rigaku.com/en>).

### Luminescence measurement

In the measurement of UCL spectra and dynamics of the samples, a photomultiplier combined with a monochromator (Andor Shamrock SR-750, <https://andor.oxinst.com/>) was used for signal collection from 300 to 750 nm. A continuous 980-nm diode laser (Hi-Tech, <http://www.htoe.com.cn/>) was used to pump the samples to investigate the steady-state spectra. In the measurements of luminescent dynamics, the samples were pumped by a tunable optical parameter oscillator (OPO, Continuum Precision II 8000). Ultraviolet-visible (UV-vis) absorption spectra were measured with a Shimadzu UV-3101PC UV-vis scanning spectrophotometer ranging of 200–1100 nm (Shimadzu, <https://www.shimadzu.com.cn/>). The emission spectra of Ru complex were recorded by F-4600 fluorescence spectrophotometer (Hitachi, <http://www.hitachi.com/>).

### Preparation of temperature and oxygen sensing system

The experimental setup for temperature sensing was composed of a test cell with holes for excitation and emission light and a circulator bath for adjusting and maintaining temperature. The nanocomposite solution was put into the testing cell, which was placed into the UCL measurement system. In our experiment, the temperature was adjusted from 10 to 50 °C, the temperature-dependency upconversion spectra were measured under the excitation of 980-nm laser.

The oxygen sensing system was integrated by a test cell with apertures for gas inlet/outlet and a gas mixer with pure nitrogen and pure oxygen cylinders for adjusting the oxygen concentration. The nanocomposite solution was put into the test cell, which was placed in the spectrophotometer. In our experiment, the oxygen concentration was adjusted from 0 to 100%, the oxygen concentration-dependency spectra were measured under the excitation of 455 nm.

### Cell imaging

Confocal imaging of cells was performed with an Olympus FV1000 CLSM (<https://www.olympus-global.com/>). The human hepatocellular carcinoma cells (HepG-2) were incubated with fresh medium containing 100  $\mu\text{g}\cdot\text{L}^{-1}$  nanocomposites for 2 h at 37 °C and washed with PBS to remove excess NPs. The 980-nm continuous-wave laser coupled to the confocal microscope provided the excitation, and the UCL emission signal was collected at  $544 \pm 10$  nm. For Ru complex imaging,

the detection scale was at  $606 \pm 10$  nm and the 455-nm laser was used as excitation source.

## Results and discussion

### Synthesis and characterization

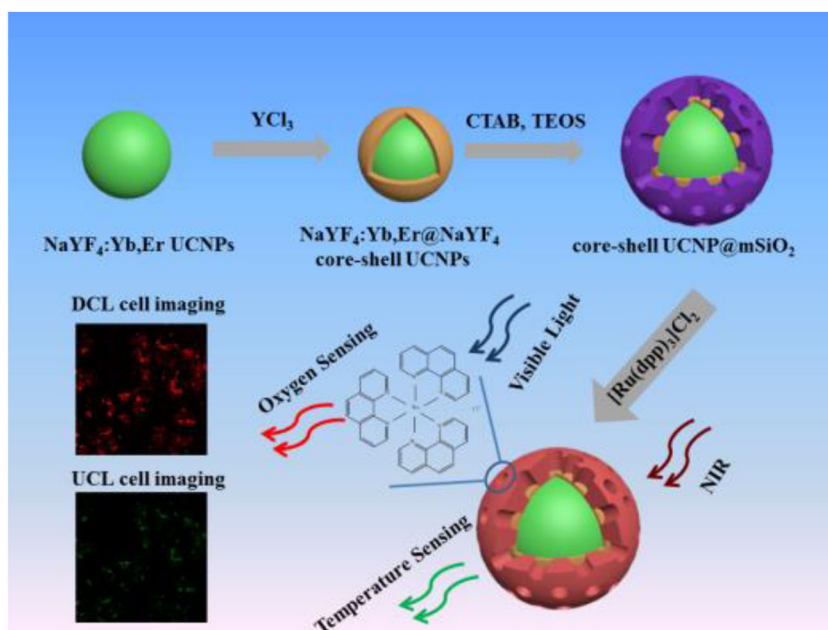
Scheme 1 illustrates the synthesis process of the nanocomposites. Hexagonal-phase  $\text{NaYF}_4\text{:Yb,Er}$  UCNPs were synthesized according to the previous method reported by Zhang's group. To obtain high efficiency of UCL, a passivation layer  $\text{NaYF}_4$  was coated on the UCNPs core to form core-shell UCNPs. Then the core-shell UCNPs were transferred to a medium by using CTAB as surfactants for the following sol-gel reaction to form mesoporous silica. Finally, CTAB surfactants were removed, thus resulting in the formation of mesoporous silica layers embedded on the surface of UCNPs. Using CTAB to transfer UCNPs into water is the key to the successful coating of mesoporous silica for obtaining monodispersed UCNPs. In this process, the hydrophobic terminal of CTAB and the hydrophobic OA ligand strongly interact, and the hydrophilic terminal of CTAB makes the UCNPs water-soluble [14]. Finally, the Ru complex embedded into the hole of the  $\text{SiO}_2$  shell.

Figures 1(a)–(c) show the TEM images of  $\text{NaYF}_4\text{:Yb,Er}$  UCNPs (referred as UCNPs below), core-shell UCNPs (referred as C/S UCNPs below), and core-shell UCNP@mSiO<sub>2</sub> (referred as UCNP@mSiO<sub>2</sub> below), respectively. It can be observed that UCNPs are well monodispersed and in uniform morphology with a size of about 17 nm (Fig. 1(a)). After coating with  $\text{NaYF}_4$  shell, the size of C/S UCNPs increase to 21 nm (Fig. 1(b)). Further coating with the mesoporous silica shell on the UCNPs, the morphological features of core-shell structure can be clearly observed. Besides, the UCNP@mSiO<sub>2</sub> shows a uniform spherical structure with a diameter of 75–80 nm (Fig. 1(c)). The XRD patterns of the three samples exhibit in Fig. 1(d). All the diffraction peaks of UCNPs and C/S UCNPs can be well attributed to hexagonal phase structure  $\text{NaYF}_4$  (JCPDS: 28–1192). The XRD pattern of UCNP@mSiO<sub>2</sub> shows a broad band centered at  $2\theta = 22^\circ$  assigned to characteristic diffraction peak of amorphous silica besides the characteristic peaks of hexagonal  $\text{NaYF}_4$ . The low angle XRD patterns of UCNP@mSiO<sub>2</sub> are shown in Fig. S1. The strong peak at  $2.3^\circ$  associated with a 2D short-range structure confirms their ordered mesostructure of shell.

### UCL and DCL properties

The UCL spectra of UCNPs, C/S UCNPs, UCNP@mSiO<sub>2</sub> and UCNP@mSiO<sub>2</sub>-Ru measured upon 980 nm excitation are shown in Fig. 2 (a). Using the approximate equally nanoparticle concentration, upconversion enhancement of 7.7

**Scheme 1** Schematic illustration of the synthesis of nanocomposites and their applications in temperature detection, oxygen sensing and dual mode cell imaging



times are obtained for NaYF<sub>4</sub>:Yb,Er UCNP after coating with an undoped NaYF<sub>4</sub> layer. However, for UCNP@mSiO<sub>2</sub> and UCNP@mSiO<sub>2</sub>-Ru, the upconversion intensities of 38.9 and 31.5% versus C/S UCNP are obtained. To further understand the cause of luminescence intensity changes, UCL dynamic processes of the transition <sup>4</sup>S<sub>3/2</sub>-<sup>4</sup>I<sub>15/2</sub> for Er<sup>3+</sup> in these four samples were observed at room temperature. It can be seen from Fig. 2(b), the emission intensities for all the samples decay monotonously with time, and the fluorescence lifetime

constants are deduced to be 172.7, 277.6, 272.7 and 271.8 μs for UCNP, C/S UCNP, UCNP@mSiO<sub>2</sub> and UCNP@mSiO<sub>2</sub>-Ru, respectively.

The large vibrational energies originate from the groups -OH and -COOH adhered on the surface of the UCNP play an important role in increasing the nonradiative relaxation process of emission centers, which lead to the quenching of UCL [15]. So the shield of the NaYF<sub>4</sub> shell leads to the UCL enhancement and the fluorescence lifetime prolongation of Er<sup>3+</sup> in C/S

**Fig. 1** TEM images of (a) UCNP, (b) C/S UCNP, (c) UCNP@mSiO<sub>2</sub> and (d) corresponding XRD patterns with the standard cards for β-NaYF<sub>4</sub> for comparison. Scale bar: 100 nm

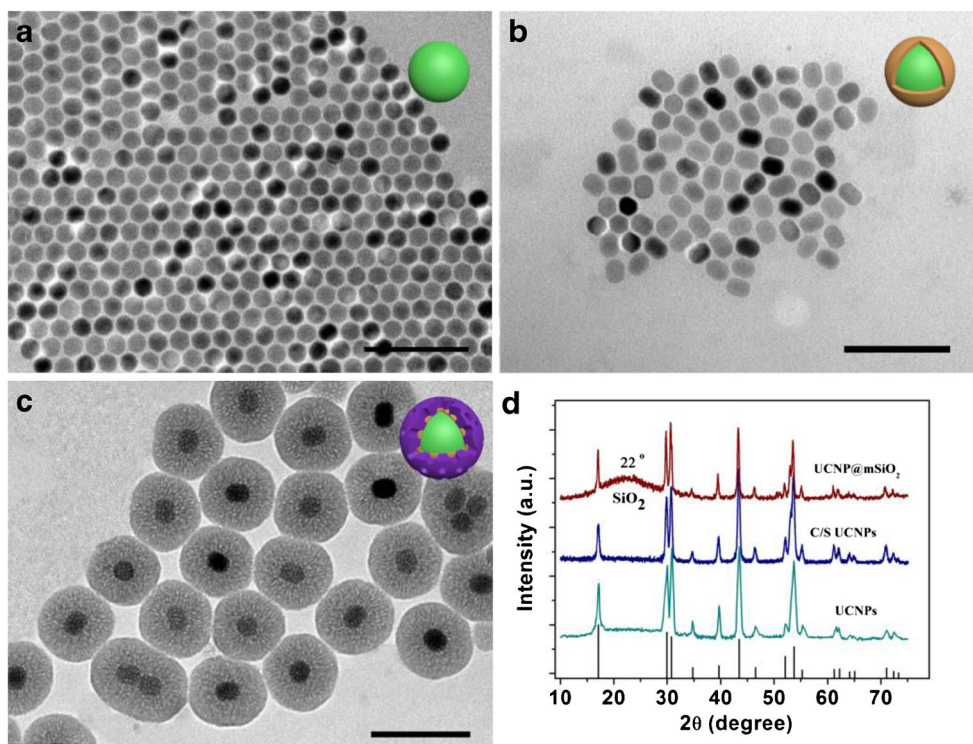
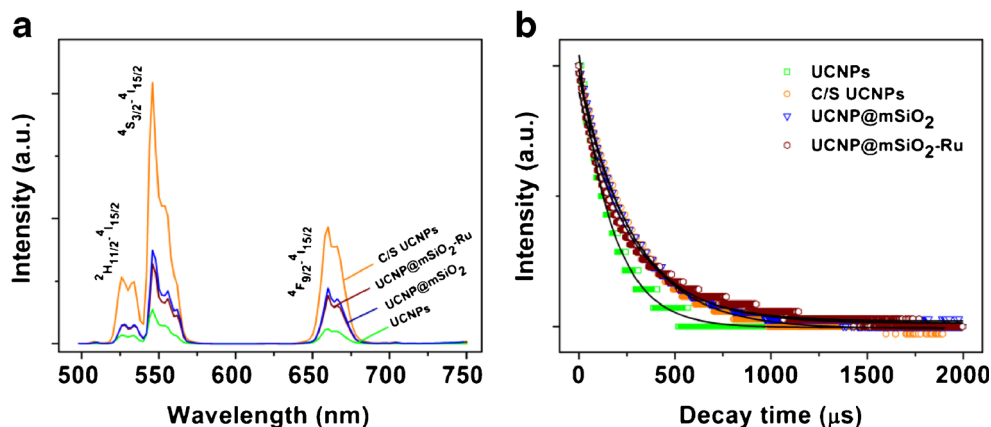




**Fig. 2** (a) UCL spectra and (b) dynamic curves for  $^4S_{3/2}$ - $^4I_{15/2}$  of  $Er^{3+}$  transition of UCNPs, C/S UCNPs, UCNP@mSiO<sub>2</sub> and UCNP@mSiO<sub>2</sub>-Ru under excitation of 980-nm laser



UCNPs [16]. After being coated with a silica layer and loaded with Ru complex, the fluorescence decrease to some extent because of the light-scattering effect on both incident and emissive lights by the silica layer [17]. In addition, the high concentration of basic solution with surfactant used in the preparation process may also damage the fluorescence core of UCNPs. The UV-vis absorption spectra of UCNP@mSiO<sub>2</sub>, Ru complex and UCNP@mSiO<sub>2</sub>-Ru are shown in Fig. S2. There is no obvious absorption peak in the absorption spectrum of UCNP@mSiO<sub>2</sub>. After loading with Ru complex, the spectrum shows an intense absorption band ranging from 350 to 550 nm, centered at 450 nm. The band assigned to the metal to ligand charge transfer (MLCT) transition ( $t_{2g} - \pi^*(bpy)$ ) of Ru complex [18]. The location of absorption band shows no significant difference from those of the pure Ru complex, indicating that there is almost no interaction between the complex and the UCNPs in the energetic ground state.

The emission spectra of UCNP@mSiO<sub>2</sub>, Ru complex and UCNP@mSiO<sub>2</sub>-Ru upon excitation of 455 nm are shown in Fig. S3. UCNP@mSiO<sub>2</sub> is found to be no emission peak upon 455 nm excitation. Ru complex and UCNP@mSiO<sub>2</sub>-Ru both show the emission band centered at 606 nm arising from ligand to metal charge-transfer excited state of Ru complex.

### Temperature sensing properties

In general, rare earth doped nanoparticles own large Stokes' shift, long fluorescence lifetime, which make such materials promising candidates for fluorescence sensing.  $Er^{3+}$  doped materials are commonly used as temperature probes because the ratio between two green emissions is a crucial parameter to calibrate temperature change. Nowadays, plenty of literatures have reported the temperature sensing property of  $Er^{3+}$  doped materials, however, these achievements mainly concentrated on the properties of the powder materials in high temperature range (300 K–900 K) [6, 19]. There are few literatures correlated to the properties of the solution state nanoparticles in the physiology temperature range. Here, we have exploited the UC temperature sensing property of the nanocomposites,

especially in the physiological range (25–45 °C). Figure 3(a) shows the UCL spectra of nanocomposites measured at temperature ranging from 10 to 50 °C. The intensity ratio  $R_{HS}$  of  $^2H_{11/2}$ - $^4I_{15/2}$  to  $^4S_{3/2}$ - $^4I_{15/2}$  increases with elevating temperature. It can be deduced that the elevated temperature leads to the population from  $^4S_{3/2}$  to  $^2H_{11/2}$ , and a quasi-thermal equilibrium is established among these two levels. According to the Boltzmann distribution law, the green emission intensity ratio  $R_{HS}$  and temperature can be expressed by the following equation [19]:

$$R_{HS} = C \exp\left(\frac{-\Delta E}{KT}\right) \quad (1)$$

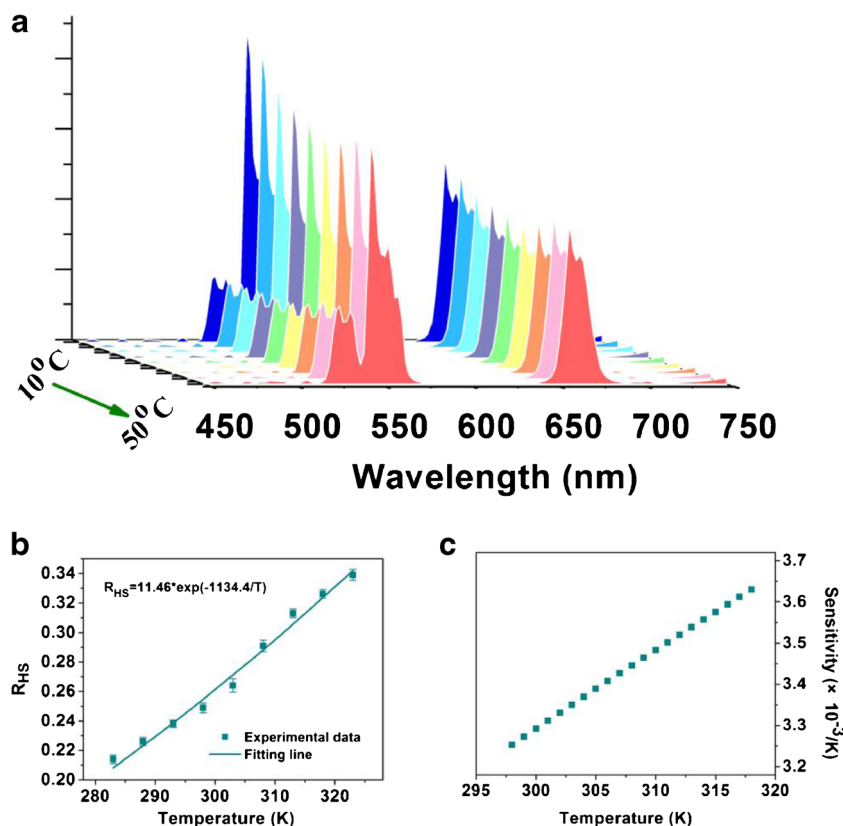
where  $C$  is a constant,  $\Delta E$  is the energy gap of the two excited states,  $k$  is Boltzmann constant, and  $T$  is absolute temperature. The solid squared dots in Fig. 3(b) show the relationship between two green emission integral intensity ratio ( $R_{HS}$ ) of 500–540 nm to 540–600 nm under the excitation of 980 nm and the temperature in the range of 283 K–323 K (10–50 °C). As the temperature rises from 10 to 50 °C, the  $R_{HS}$  value increases from 0.214 to 0.339. Equation (1) was used to fit the experimental dots. From the fitting results, the values of the parameters  $C$  and  $\frac{\Delta E}{K}$  were confirmed to be 11.46 and 1134.4 K with small uncertainties. These results obtained in this work are similar to those in former literatures [6, 19]. This indirectly demonstrates that the population distribution of the two green levels in the nanocomposite system we established follows the Boltzmann law, and the temperature sensing based on the intensity ratio is applicable.

For temperature sensing, sensitivity is also an important factor to evaluate the performance of the sensor. For  $Er^{3+}$  doped temperature sensor, the sensitivity can be defined as [6, 19]:

$$S = \frac{dR}{dT} = C \exp\left(-\frac{\Delta E}{KT}\right) \left(\frac{\Delta E}{KT^2}\right) \quad (2)$$

From the equation, it can be seen that the sensitivity  $S$  is dependence on the temperature. By taking the above fitted

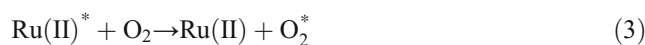
**Fig. 3** (a) UCL spectra of nanocomposites excited at 980 nm in a temperature region of 10–50 °C (283–323 K), (b) relationship between two green emission integral intensity ratio of 500–540 nm to 540–600 nm and temperature ranging from 10 to 50 °C (283–323 K), (c) sample temperature sensitivity curve of nanocomposites ranging from 25 to 45 °C (298–318 K)



values of  $C$  and  $\frac{\Delta E}{K}$  into eq. (2), the sensitivity curve in the physiological temperature range of 298–318 K (25–45 °C) with the interval of 1 degree was plotted in Fig. 3(c). The sensitivity of the nanocomposites ranges from 0.00325–0.00363 K<sup>-1</sup> in this temperature range, and the sensitivity increases with the increasing of the temperature. It should be pointed that the constant  $C$  is proportional to the ratio of spontaneous emission rates of <sup>2</sup>H<sub>11/2</sub> to <sup>4</sup>S<sub>3/2</sub>. Higher doping concentration of Er<sup>3+</sup> can lead to the decrease of the ratio, so the lower doping concentration may obtain higher green emission intensity ratio and detection sensitivity [20, 21]. Apart from the nanocomposites established in this work, other materials, including quantum dots, organic fluorophores, rare-earth metal complex, and inorganic materials, also can act as thermometers. Compared to five other reported thermometers, the new probe shows a suitable sensitivity, as shown in Table 1.

### Oxygen sensing behaviors

To determine the oxygen-sensitive performance of the nanocomposite, the emission spectra were recorded under different concentrations of O<sub>2</sub>. As shown in the inset of Fig. 4(a), the luminescence intensity decreases as the increasing of the oxygen concentrations. The quenching process of Ru complex by oxygen can be expressed as follows [18]:



where Ru(II) represents Ru complex and \* denotes the excited state.

For Ru complex, the optimum absorption wavelength is around 450 nm. The most suitable laser coupled with confocal laser scanning microscopy is 455 nm. To maintain the

**Table 1** Different luminescence probes for thermal sensing

Thermometer	Temperature range[°C]	Sensitivity [1/°C]	Ref.
CdSeQDs	30–60	0.015%	[22]
DyLight 549	25–42	1.5%	[23]
Eu-TTA@polymer NPs	20–60	2.2%	[24]
NaYF <sub>4</sub> :Er <sup>3+</sup> ,Yb <sup>3+</sup> NPs	10–36	1.6%	[25]
NaGdF <sub>4</sub> :Nd <sup>3+</sup> NPs & QDs @PLGA	10–50	0.025%	[26]
mSiO <sub>2</sub> coating UCNPs loaded with Ru complex	25–40	0.036%	This work

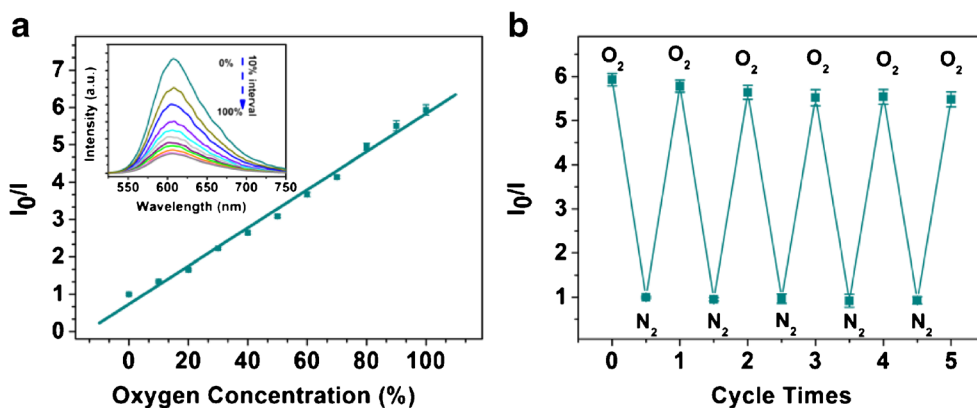


**Fig. 4** (a) Stern-Volmer plot of emission integrated intensity ratio of 525–750 nm for nanocomposites at different concentrations of dissolved oxygen upon excitation of 455 nm, (b) luminescent emission responses

of nanocomposites to  $N_2$ - $O_2$  cycles (inset of Fig. 4(a): emission spectra of nanocomposites under different oxygen concentrations upon excitation of 455 nm)

excitation wavelength consistent, 455 nm was selected as excitation wavelength in the oxygen sensing and downconversion imaging experiment. When Ru complex is irradiated upon 455-nm light, Ru(II) is excited to the excited state Ru(II)\*. When the Ru(II)\* is exposure to oxygen, energy transfer occurs from Ru(II)\* to  $O_2$ , leading to the luminescence quenching of Ru complex. The extent of quenching of Ru complex is dependent on the oxygen concentration, and can be described by Stern-Volmer equation [18]:

$$\frac{I_0}{I} = 1 + K_{sv}[Q] \quad (4)$$

where  $I$  and  $I_0$  represent the luminescence intensities of Ru complex in the presence and absence of  $O_2$ , respectively,  $K_{sv}$  is the Stern-Volmer constant, and  $[Q]$  is the oxygen concentration. As shown in the Fig. 4(a), the plot of emission integrated intensity ratio ( $I_0/I$ ) of 525–750 nm under the excitation of 455 nm versus oxygen concentrations shows a good linear relationship ( $R^2 = 0.9948$ ) in the oxygen concentration range (0–100%), and the  $K_{sv}$  is found to be  $4.939 O_2\%^{-1}$ . The detection limit of the sensor is defined as  $3\sigma/m$ , and calculated to be 1.32%.  $\sigma$  is obtained from the standard deviation of the intensity peak recorded of the nanocomposites at 0% oxygen (100% nitrogen) and  $m$  is the slope of the calibration plot. For convenience of comparison,  $I_0/I_{100}$  is defined as oxygen sensitivity, where  $I_0$  is the emission intensity under 100%  $N_2$  atmosphere, and  $I_{100}$  is that under 100%  $O_2$  atmosphere. The value of  $I_0/I_{100}$  in our system is achieved as

5.8. Table 2 compares the performance of several known oxygen probes with the new probe, revealing that the latter exhibits relatively higher sensitivity.

For an oxygen sensor, reversibility is also important in practical applications, especially for the dynamic monitoring of oxygen concentration in living cells. Figure 4(b) shows the signal changes of the nanocomposites when switching between pure  $N_2$  and pure  $O_2$  atmosphere. The cycles are reversible and are repeated for at least five times with only a slightly luminescence decrement (8.3% bleaching during cycling). It should be pointed that the reaction of  $O_2$  in the air and nanocomposites in preparation process and conservation is inevitable. The reversibility also can ensure the detection results are not affected by the  $O_2$  in the air reacted with the nanocomposites in the preparation. However, the major limitation for oxygen sensing is the excitation light is 455 nm. Blue light has limitation penetration depth, and may cause damage to cells under long-term excitation. We intend to perform further work on UCNPs loaded with other oxygen sensitive dyes that can be excited by red or near infrared light.

## Dual-mode cell imaging

For the application of intracellular detection, the probes should have the function of cell imaging. So far, a lot of fluorescent probes have been explored for fluorescent bioimaging [30, 31]. The nanocomposites also have the functions for

**Table 2** Different luminescence probes for oxygen sensing

Materials	$\lambda_{exc/em}$ [nm]	Sensitivity	Ref.
mSiO <sub>2</sub> coating Fe <sub>3</sub> O <sub>4</sub> loaded with Ru complex	365/612	5.53 ( $I_0/I_{100}$ )	[9]
Dy complex	300/537	1.9 ( $I_0/I_{100}$ )	[27]
UCNPs and PtTPTBP dyes	980/600	1.8 ( $I_0/I_{air-1}$ )	[28]
Eu doped Y <sub>2</sub> O <sub>3</sub> nanosheets	356/614	2.8 ( $I_0/I_{100}$ )	[29]
mSiO <sub>2</sub> coating UCNPs loaded with Ru complex	455/606	5.8 ( $I_0/I_{100}$ )	This work

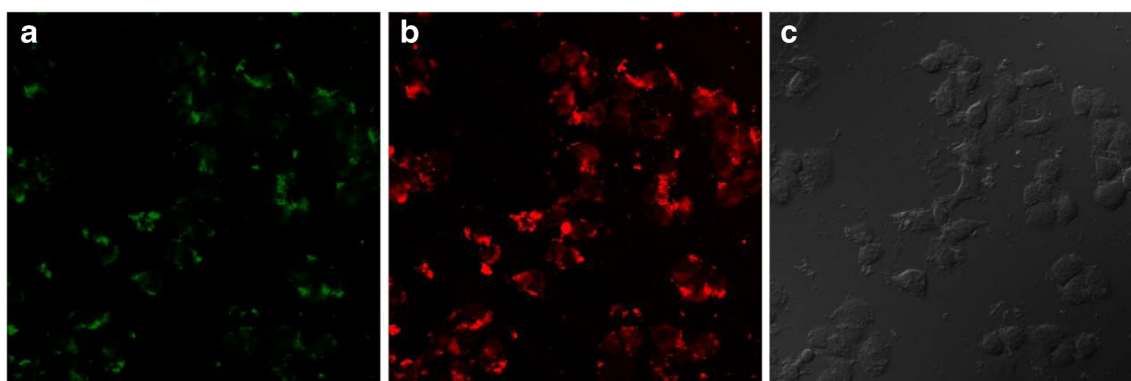


**Fig. 5** (a,b) CLSM images and (c) bright field image of fixed HepG2 cells with (a) 980 nm excitation and (b) 455 nm excitation. Fluorescence images of cells were measured at 534–554 nm for UCL from  $\text{Er}^{3+}$  and 596–616 nm for DCL from Ru complex

upconversion and downconversion cell imaging based on their UCL and DCL under near infrared and visible light excitation, respectively. For upconversion bioimaging, 808-nm light is mostly used as excitation source due to its weaker heat effect than that of 980 nm.  $\text{Nd}^{3+}$  exhibits considerable absorption and cross-sectional area in the 808 nm region, so  $\text{Nd}^{3+}$  is usually used as sensitizer. However, although the  $\text{Nd}^{3+}$  ion can directly transfer energy to activators ( $\text{Er}^{3+}$ ,  $\text{Tm}^{3+}$ ,  $\text{Ho}^{3+}$ ), its transfer efficiency is low. To solve this problem,  $\text{Yb}^{3+}$  ion is added as medium. Under excitation of 808 nm,  $\text{Nd}^{3+}$  ions transfer excitation energy to nearby  $\text{Yb}^{3+}$  ions, which in turn serve as energy migrators that transfer energy to emitting ions, resulting in UC emission. The two-step energy process from  $\text{Nd}^{3+}$  ions to activators inevitably consumes a large amount of harvesting excitation energy absorbed by  $\text{Nd}^{3+}$  [32]. In addition, unlike  $\text{Yb}^{3+}$ ,  $\text{Nd}^{3+}$  has multiple energy levels, which result in deleterious cross-relaxation between the activators [33]. All of these will result in low luminescence efficiency of  $\text{Nd}^{3+}$  doped UCNPs excited by 808 nm. Low luminescence efficiency will affect the temperature detection sensitivity and cell imaging based on upconversion emission. So, we selected 980-nm laser as excitation source instead of 808 nm.

Herein, HepG-2 cells were used to investigate the dual mode cell imaging functions. Fig. 5(a) and (b) shows the

confocal images upon 980-nm and 455-nm lasers irradiation, respectively, and Fig. 5(c) displays the bright field image of cells after incubation with the nanocomposites. As shown in Fig. 5, the green image from UCL of  $\text{Yb}^{3+}/\text{Er}^{3+}$  ions and the red image from DCL of Ru complex can fit well with each other. The dual-mode imaging results confirm that we can achieve both UCL and DCL using one boilable. In addition, if  $\text{Er}^{3+}$  is replaced by  $\text{Ho}^{3+}$ , a highly paramagnetic lanthanide ion, the nanocomposites may possess magnetic resonance imaging function, except for fluorescence imaging. [34, 35]

### Cytotoxicity assay

Low cell toxicity is one of the important indicators for a bio-sensor using in living cells. The MTT assay was performed to investigate the cytotoxicity of the nanocomposites in this work. HepG-2 cells were incubated with different concentrations of nanocomposite solution in the range of 0 to 200  $\mu\text{g}\cdot\text{mL}^{-1}$ . As shown in Fig. 6, the cellular viabilities maintain over 85% after co-incubation 24 h. Our in vitro cytotoxicity study confirms that the nanocomposites have relatively low cytotoxicity, making them potentially available for luminescence bio-sensing and imaging in vitro.

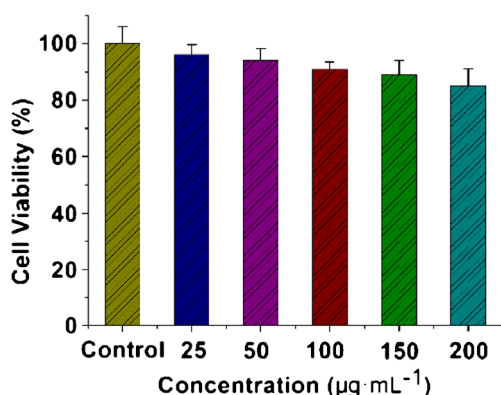


**Fig. 6** In vitro cell viabilities of HepG2 cells incubated with nanocomposites at different concentrations for 24 h

### Conclusion

In this work, we have successfully developed multifunctional nanocomposites based on mesoporous capping upconversion nanoparticles by loading Ru complex, the UCNP@mSiO<sub>2</sub>-Ru can achieve three functions: (i) temperature sensing properties through the readout luminescence ratio from  $\text{Er}^{3+}$  in the range of 10–50 °C with a good linear relationship ( $R^2 = 0.9948$ ) and relatively high sensitivity in the physiological temperature range of 25–40 °C, (ii) oxygen sensing behaviors with a good Stern-Volmer characteristic between the luminescence intensity of Ru complex and the concentrations of oxygen (0–100%), (iii) dual mode cell imaging of DCL and UCL under



the excitation of 455-nm light and 980-nm laser, respectively. In this system, the temperature and oxygen-sensing properties have been performed upon different wavelengths excitation to avoid the disturbances of each other. Generally, the UCNP@mSiO<sub>2</sub>-Ru nanocomposites can serve as promising candidates for temperature and oxygen sensing at cellular level. This work provides a new insight into developing upconversion and downconversion nanocomposites for multifunctional biomedical applications.

**Acknowledgements** This work is supported by National Natural Science Foundation of China (11704056, 11774042), Fundamental Research Funds for the Central Universities (3132018244, 3132016333), China Postdoctoral Science Foundation (2018 T110212, 2016 M591420), Key Scientific and Technological Research Projects in Henan Province (152102210217), and Key Research Foundation of the Higher Education Institutions of Henan Province (16A510008).

**Compliance with ethical standards** The author (s) declare that they have no competing interests.

## References

- Liu J, Liu Y, Bu W, Bu J, Sun Y, Du J, Shi J (2014) Ultrasensitive nanosensors based on upconversion nanoparticles for selective hypoxia imaging in vivo upon near-infrared excitation. *J Am Chem Soc* 136:9701–9709
- Hockel M, Schlenger K, Knoop C, Vaupel P (1991) Oxygenation of carcinomas of the uterine cervix: evaluation by computerized O<sub>2</sub> tension measurements. *Cancer Res* 51:6098–6102
- Bai T, Gu N (2016) Micro/nanoscale thermometry for cellular thermal sensing. *Small* 12:4590–4610
- Zheng W, Huan P, Tu D, Ma E, Zhu H, Chen X (2015) Lanthanide-doped upconversion nano-bioprobes: electronic structures, optical properties, and biodetection. *Chem Soc Rev* 44:1379–1415
- Sedlmeier A, Achatz DE, Fischer LH, Gorris HH, Wolfbeis OS (2012) Photon upconverting nanoparticles for luminescent sensing of temperature. *Nanoscale* 4:7090–7096
- Du P, Yu J (2018) Synthesis of Er (III)/Yb (III)-doped BiF<sub>3</sub> upconversion nanoparticles for use in optical thermometry. *Microchim Acta* 185:237
- Wang XD, Wolfbeis OS (2014) Optical methods for sensing and imaging oxygen: materials, spectroscopies and applications. *Chem Soc Rev* 43:3666–3761
- Fischer LH, Borisov SM, Schaeferling M, Klimant I, Wolfbeis OS (2010) Dual sensing of pO<sub>2</sub> and temperature using a water-based and sprayable fluorescent paint. *Analyst* 135:1224–1229
- Li JJ, Yang CJ, Wu YZ, Wang BR, Sun WH, Shao TF (2016) On a magnetic-mesoporous composite loaded with emissive Ru(II) complex for oxygen sensing application: Construction, characterization and emission response to oxygen molecules. *Inorg Chim Acta* 442: 111–118
- Wang M, Abbineni G, Clevenger A, Mao CB, Xu SK (2011) Upconversion nanoparticles: synthesis, surface modification and biological applications. *Nanomed Nanotechnol Biol Med* 7:710–729
- Sun L, Ge X, Liu J, Qiu Y, Wei Z, Tian B, Shi L (2014) Multifunctional nanomesoporous materials with upconversion (in vivo) and downconversion (in vitro) luminescence imaging based on mesoporous capping UCNPs and linking lanthanide complexes. *Nanoscale* 6:13242–13252
- Li Z, Zhang Y (2008) An efficient and user-friendly method for the synthesis of hexagonal-phase NaYF<sub>4</sub>:Yb,Er/Tm nanocrystals with controllable shape and upconversion fluorescence. *Nanotechnology* 19:345606
- Li CX, Hou Z, Dai Y, Yang D, Cheng Z, Ma PA, Lin J (2013) A facile fabrication of upconversion luminescent and mesoporous core-shell structured beta-NaYF<sub>4</sub>:Yb<sup>3+</sup>, Er<sup>3+</sup>@mSiO<sub>2</sub> nanocomposite spheres for anti-cancer drug delivery and cell imaging. *Biomater Sci* 1:213–223
- Meng H, Yang S, Li Z, Xia T, Chen J, Ji Z, Zhang H, Wang X, Lin S, Huang C, Zhou ZH, Zink JI, Nel AE (2011) Aspect ratio determines the quantity of mesoporous silica nanoparticle uptake by a small GTPase-dependent macropinocytosis mechanism. *ACS Nano* 5:4434–4447
- Bai X, Song H, Pan G, Lei Y, Wang T, Ren X, Lu S, Dong B, Dai Q, Fan L (2007) Size-dependent upconversion luminescence in Er<sup>3+</sup>/Yb<sup>3+</sup>-codoped nanocrystalline yttria: Saturation and thermal effects. *J Phys Chem C* 111:13611–13617
- Yi GS, Chow GM (2007) Water-soluble NaYF<sub>4</sub>:Yb,Er (Tm)/NaYF<sub>4</sub>/polymer core/shell/shell nanoparticles with significant enhancement of upconversion fluorescence. *Chem Mater* 19:341–343
- Li ZQ, Wang LM, Wang ZY, Liu XH, Xiong YJ (2011) Modification of NaYF<sub>4</sub>:Yb,Er@SiO<sub>2</sub> nanoparticles with gold nanocrystals for tunable green-to-red upconversion emissions. *J Phys Chem C* 115:3291–3296
- Wang Y, Li B, Zhang L, Song H (2013) Multifunctional mesoporous nanocomposites with magnetic, optical, and sensing features: synthesis, characterization, and their oxygen-sensing performance. *Langmuir* 29:1273–1279
- Xu S, Xiang S, Zhang Y, Zhang J, Li X, Sun J, Cheng L, Chen B (2017) 808 nm laser induced photothermal effect on Sm<sup>3+</sup>/Nd<sup>3+</sup> doped NaY (WO<sub>4</sub>)<sub>2</sub> microstructures. *Sens Actuators B: Chem* 240:386–391
- Liu L, Sun ZS, Ma C, Tao RX, Zhang JZ, Li HY, Zhao EM (2018) Highly sensitive and accurate optical thermometer through Er doped tellurite glasses. *Mater Res Bull* 105:306–311
- Li XP, Wang X, Zhong H, Cheng LH, Xu S, Zhang JS, Li XJ, Tong LL, Chen BJ (2016) Effects of Er<sup>3+</sup> concentration on down-/up-conversion luminescence and temperature sensing properties in NaGdTiO<sub>4</sub>: Er<sup>3+</sup>/Yb<sup>3+</sup> phosphors. *Ceram Int* 42:14710–14715
- Maestro LM, Haro-Gonzalez P, del Rosal B, Ramiro J, Caamano AJ, Carrasco E, Juarranz A, Sanz-Rodriguez F, Sole JG, Jaque D (2013) Heating efficiency of multi-walled carbon nanotubes in the first and second biological windows. *Nanoscale* 5:7882–7889
- Huang H, Delikanli S, Zeng H, Ferkey DM, Pralle A (2010) Remote control of ion channels and neurons through magnetic-field heating of nanoparticles. *Nat Nanotechnol* 5:602–606
- Oyama K, Takabayashi M, Takei Y, Arai S, Takeoka S, Ishiwata S, Suzuki M (2012) Walking nanothermometers: spatiotemporal temperature measurement of transported acidic organelles in single living cells. *Lab Chip* 12:1591–1593
- Rodríguez-Sevilla P, Zhang Y, Haro-González P, Sanz-Rodríguez F, Jaque F, Solé JG, Liu X, Jaque D (2016) Thermal scanning at the cellular level by an optically trapped upconverting fluorescent particle. *Adv Mater* 28:2421–2426
- Cerón EN, Ortigies DH, del Rosal B, Ren F, Benayas A, Vetrone F, Ma D, Sanz-Rodríguez F, Solé JG, Jaque D (2015) Hybrid nanostructures for high-sensitivity luminescence nanothermometry in the second biological window. *Adv Mater* 27:4781–4787.
- Nakai H, Seo J, Kitagawa K, Goto T, Matsumoto T, Ogo S (2016) An oxygen-sensitive luminescent Dy(III) complex. *Dalton Trans* 45:9492–9496
- Scheucher E, Wilhelm S, Wolfbeis OS, Hirsch T, Mayr T (2015) Composite particles with magnetic properties, near-infrared

- excitation, and far-red emission for luminescence-based oxygen sensing. *Microsyst Nanoeng* 1:15026
29. Yang W, Xia JF, Zhou GH, Jiang DY, Li Q, Wang SW, Zheng XH, Li X, Xin L, Shen YB (2018) Luminescent oxygen-sensing film based on beta-diketone-modified Eu (III)-doped yttrium oxide nanosheets. *Sens Actuators B* 257:340–346
  30. Zhou J, Zhou H, Tang JB, Deng S, Yan F, Li WJ, Qu MH (2017) Carbon dots doped with heteroatoms for fluorescent bioimaging: a review. *Microchim Acta* 184:343–368
  31. Zhou H, Tang JB, Lv LL, Sun N, Zhang J, Chen BC, Mao J, Zahng WF, Zhang J, Zhou J (2018) Intracellular endogenous glutathione detection and imaging by a simple and sensitive spectroscopic off-on probe. *Analyst* 143:2390–2396
  32. Chang MH, Liu RS (2017) Advanced sensing, imaging, and therapy nanoplatforms based on Nd<sup>3+</sup>-doped nanoparticle composites exhibiting upconversion induced by 808 nm near-infrared light. *Nanoscale* 9:18153–18168
  33. Wang D, Xue B, Song J, Qu JL (2018) Compressed energy transfer distance for remarkable enhancement of the luminescence of Nd<sup>3+</sup>-sensitized upconversion nanoparticles. *J Mater Chem C* 6:6597–6604
  34. Syamchand SS, Aparna RS, Sony G (2017) Plasmonic enhancement of the upconversion luminescence in a Yb<sup>3+</sup> and Ho<sup>3+</sup> codoped gold-ZnO nanocomposite for use in multimodal imaging. *Microchim Acta* 184:2255–2264
  35. Syamchand SS, Sony G (2016) Fluorescein-labeled fluoroapatite nanocrystals codoped with Yb (III) and Ho (III) for trimodal (downconversion, upconversion and magnetic resonance) imaging of cancer cells. *Microchim Acta* 183:3209–3219